AMSE JOURNALS –2015-Series: Modelling B; Vol. 84; N° 1; pp 1-22
Submitted Aug. 2014; Revised Feb. 2, 2015; Accepted Feb. 28, 2015

Unsteady Casson Fluid Flow through Parallel Plates with Hall Current, Joule Heating and Viscous Dissipation

*Md. Faisal Kabir, **Md. Mahmud Alam

*Mathematics, Science, Engineering and Technology School, Khulna University
Khulna - 9208, Bangladesh, (faisalkabir08ku@gmail.com)
** Mathematics, Science, Engineering and Technology School, Khulna University
Khulna - 9208, Bangladesh, (alam_mahmud2000@yahoo.com)

Abstract

The unsteady magnetohydrodynamic flow of an electrically conducting viscous incompressible non-Newtonian Casson fluid bounded by two parallel non-conducting porous plates has been studied with Hall current, Joule heating and Viscous dissipation The developed model has been dimenssionalized by usual transformation technique. The obtained non-similar coupled non-linear partial differential equations have been solved by using explicit finite difference technique. The primary and secondary velocity profiles and temperature distributions are discussed for the different values of dimensionless parameter verses dimensionless coordinate. The shear stress and Nusselt number have also been investigated. The obtained results have been discussed with the help of graphs to observe effects of various parameters on the above mentioned quantities. The stability conditions and convergence criteria of the explicit finite difference scheme are established for finding the restriction of the values of various parameters to get more accuracy.

Key words

Casson fluid, Hall current, Joule heating and Viscous dissipation

1. Introduction

In fluid dynamics, Couette flow is the laminar flow of a viscous fluid in the space between two parallel plates, one of which is moving relative to the other. The flow is driven by virtue of viscous drag force acting on the fluid and the applied pressure gradient parallel to the plates. The magnetohydrodynamic (MHD) flow between two parallel plates, one in uniform motion and the

other held at rest known as MHD Couette flow, is a classical problem that has many applications in MHD power generators and pumps, accelerators, aerodynamic heating, electrostatic precipitation, polymer technology, petroleum industry, purification of crude oil and fluid droplets and sprays, electrostatic precipitation, polymer technology, flow meters and nuclear reactors using liquid metal coolants. The most important non-Newtonian fluid possessing a yield value is the Casson fluid, which has significant applications in polymer processing industries and biomechanics. Casson fluid is a shear thinning liquid which has an infinite viscosity at a zero rate of shear, a yield stress below which no flow occurs and a zero viscosity at an infinite rate of shear such as Nail polish, whipped cream, ketchup, molasses, syrups, paper pulp in water, latex paint, ice, blood, some silicone oils, some silicone coatings. Casson's constitutive equation represents a nonlinear relationship between stress and rate of strain and has been found to be accurately applicable to silicon suspensions, suspensions of bentonite in water and lithographic varnishes used for printing inks Casson [1] and Walawander et al. [2]. Batra and Jena [3], Das and Batra [4], Sayed-Ahmed and Attia [5] and Attia [6] have analyzed the flow or/and heat transfer of a Casson fluid in different geometries. Sahoo et al. [7] have studied the MHD mixed convection stagnation point flow and heat transfer in a porous medium. Panda et al. [8] have analyzed heat and mass transfer on MHD flow through porous media over an accelerating surface in the presence of suction and blowing. Panda et al. [9] have studied hydromagnetic flow and heat transfer through porous medium of elasto-viscous fluid over a porous plate in the slip flow regime. Attia [10] has studied the influence of the Hall current on the velocity and temperature fields of an unsteady Hartmann flow of a conducting Newtonian fluid between two infinite non-conducting horizontal parallel and porous plates. Attia and Sayed-Ahmed [11] has studied transient MHD Couette flow of a Casson fluid between parallel plates with heat transfer. Sayed-Ahmed et al. [12] has analyzed time dependent pressure gradient effect on unsteady MHD couette flow and heat transfer of a casson fluid.

Our aim of this research is to extend the work of Attia and Sayed-Ahmed [11] in case of one dimensional flow.

In this study, the unsteady magnetohydrodynamic flow of an electrically conducting viscous incompressible non-Newtonian Casson fluid bounded by parallel non-conducting porous plates has been studied with Hall current, Joule heating and Viscous dissipation.

The governing equations of the problem contain a system of non-linear coupled partial differential equations which are transfomed by usual transformation into a non-dimensional system of partial coupled non-linear differential equations. The obtained non-similar partial

differential equations have been solved numerically by explicit finite difference technique. The primary and secondary velocity profiles and temperature distributions are discussed for the different values of dimensionless parameter verses dimensionless coordinate. The shear stress and Nusselt number have also been investigated. The results of this study are discussed for the different values of the well known parameters and are shown graphically.

2. Mathematical Model of the Flow

The fluid is assumed to be laminar, incompressible and obeying a Casson model and flows between two infinite horizontal plates located at the $y = \pm h$ planes and extend from $x = -\infty$ to ∞ and from $z = -\infty$ to ∞. The upper plate is suddenly set into motion and moves with a uniform velocity U_0 while the lower plate is stationary. The upper plate is simultaneously subjected to a step change in temperature from T_1 to T_2. Then, the upper and lower plates are kept at two constant temperatures T_1 and T_2 respectively, with $T_2 > T_1$. The fluid is acted upon by an exponentially decaying pressure gradient in the *x*-direction, and a uniform suction from above and injection from below which are applied at t = 0. A uniform magnetic field B_0 is applied in the positive *y*-direction. The physical model of this study is furnished in the following fig.1.

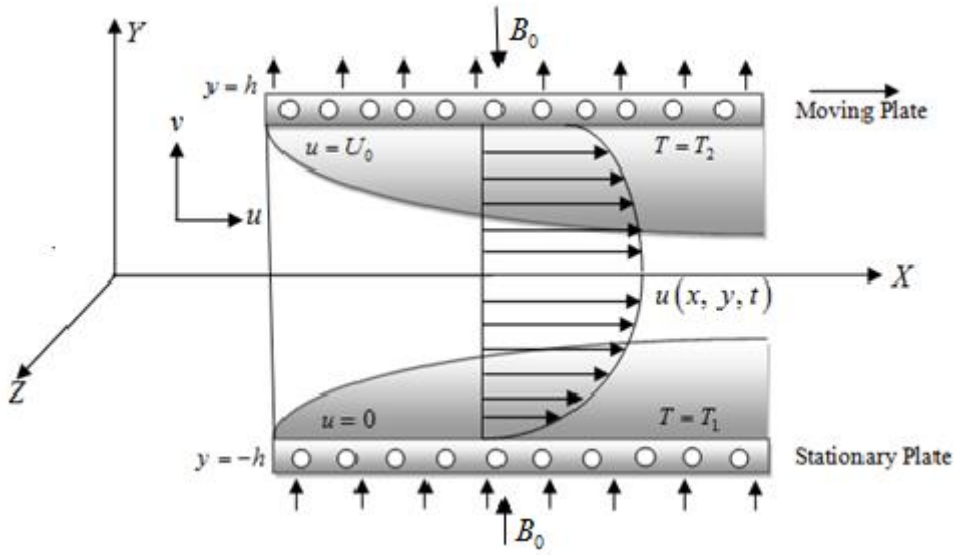

Fig. 1 Geometrical configuration of boundary layer

A uniform magnetic field is assumed undisturbed as the induced magnetic field is neglected by assuming a very small magnetic Reynolds number. The Hall effect is taken into consideration and consequently a *z*-component for the velocity is expected to arise. The uniform injection

implies that the *y*-component of the velocity v_0 is constant. The fluid motion has been started from rest at $t = 0$, and the no-slip condition at the plates in *z*-direction implies that the fluid velocity has no *z*-component at $y = \pm h$. The initial temperature of the fluid is assumed to be equal to T_1. Since the plates are infinite in the *x* and *z*- directions, the physical quantities do not change in these directions. The equation of conservation of electric charge, $\nabla.\mathbf{J} = 0$ gives $J_y = \text{constant}$ where the current density $\mathbf{J} = (J_x, J_y, J_z)$, because the direction of propagation is considered only along the *y*-axis and $\mathbf{J}$ does not have any variation along the *y*-axis. Since the plate is electrically non-conducting, the constant is zero i.e. $J_y = 0$ at the plate and everywhere.

Since the plates are infinitely extended and the fluid motion is unsteady so all the flow variables are function of y and t. Thus accordance with the above assumptions relevant to the problem and Boussinesq's approximation, the basic boundary layer equations are given below;

Continuity equation

$$\frac{\partial v}{\partial y} = 0 \tag{1}$$

Momentum equation in *x*-direction

$$\frac{\partial u}{\partial t} - v_0 \frac{\partial u}{\partial y} = -\frac{1}{\rho}\frac{\partial P}{\partial x} + \frac{1}{\rho}\left[\frac{\partial}{\partial y}\left(\mu \frac{\partial u}{\partial y}\right)\right] - \frac{1}{\rho}\left[\frac{\sigma B_0^2}{1+m^2}(u + mw)\right] \tag{2}$$

Momentum equation in *z*-direction

$$\frac{\partial w}{\partial t} - v_0 \frac{\partial w}{\partial y} = -\frac{1}{\rho}\frac{\partial P}{\partial z} + \frac{1}{\rho}\left[\frac{\partial}{\partial y}\left(\mu \frac{\partial w}{\partial y}\right)\right] - \frac{1}{\rho}\left[\frac{\sigma B_0^2}{1+m^2}(w - mu)\right] \tag{3}$$

Energy equation

$$\frac{\partial T}{\partial t} - v_0 \frac{\partial T}{\partial y} = \frac{\kappa}{\rho c_p}\frac{\partial^2 T}{\partial y^2} + \frac{\mu}{\rho c_p}\left[\left(\frac{\partial u}{\partial y}\right)^2 + \left(\frac{\partial w}{\partial y}\right)^2\right] + \frac{1}{\rho c_p \sigma}\frac{\sigma^2 B_0^2}{1+m^2}\left(u^2 + w^2\right) \tag{4}$$

Apparent viscosity

$$\mu = \left[K_c + \left(\frac{\tau_0}{\sqrt{\left(\frac{\partial u}{\partial y}\right)^2 + \left(\frac{\partial w}{\partial y}\right)^2}}\right)^{1/2}\right]^2 \tag{5}$$

with the corresponding initial and boundary conditions are;

$$t \le 0, \qquad u = 0, \qquad w = 0, \qquad T = T_1 \qquad \text{everywhere} \tag{6}$$

$$t>0, \quad u=0, \quad w=0, \quad T=T_1 \quad \text{for } y=-h$$
$$u=U_0, \quad w=0, \quad T=T_2 \quad \text{for } y=h \tag{7}$$

Where x, y are cartesian coordinate system; u, v are x, y component of flow velocity respectively; υ is the kinematic viscosity; ρ is the density of the fluid; m is the Hall parameter; σ is the electrical conductivity; κ is the thermal conductivity; c_p is the specific heat at the constant pressure; K_c^2 is the Casson's coefficient of viscosity; τ_0 is the yield stress; μ is the apparent viscosity.

3. Mathematical Formulation

Since the governing equations (1)-(5) under the initial (6) and boundary (7) conditions have been based on the finite difference technique it is required to make these equations dimensionless. For this purpose the following dimensionless quantities are introduceed;

$$X=\frac{x}{h}, \quad Y=\frac{y}{h}, \quad U=\frac{u}{U_0}, \quad W=\frac{w}{U_0}, \quad \tau=\frac{tU_0}{h}, \quad P=\frac{p}{\rho U_0^2}, \quad \theta=\frac{T-T_1}{T_2-T_1} \quad \text{and} \quad \bar{\mu}=\frac{\mu}{K_0^2}.$$

The above dimensionless variables become;

$$x=hX, \quad y=hY, \quad u=U_0U, \quad w=U_0W, \quad t=\frac{\tau h}{U_0}, \quad p=\rho U_0^2P, \quad T=T_1+(T_2-T_1)\theta$$

and $\mu=K_0^2\bar{\mu}$.

Now the values of the above derivatives are substituted into the equations (1)-(5) and after simplification the following nonlinear coupled partial differential equations interms of dimensionless variables are obtained;

$$\frac{\partial V}{\partial Y}=0 \tag{8}$$

$$\frac{\partial U}{\partial \tau}-\frac{S}{R_e}\frac{\partial U}{\partial Y}=-\frac{dP}{dX}+\frac{1}{R_e}\left[\frac{\partial}{\partial Y}\left(\bar{\mu}\frac{\partial U}{\partial Y}\right)-\frac{H_a^2}{1+m^2}(U+mW)\right] \tag{9}$$

$$\frac{\partial W}{\partial \tau}-\frac{S}{R_e}\frac{\partial W}{\partial Y}=\frac{1}{R_e}\left[\frac{\partial}{\partial Y}\left(\bar{\mu}\frac{\partial W}{\partial Y}\right)-\frac{H_a^2}{1+m^2}(W-mU)\right] \tag{10}$$

$$\frac{\partial \theta}{\partial \tau}-\frac{S}{R_e}\frac{\partial \theta}{\partial Y}=\frac{1}{P_r}\frac{\partial^2\theta}{\partial y^2}+E_c\,\bar{\mu}\left[\left(\frac{\partial U}{\partial Y}\right)^2+\left(\frac{\partial W}{\partial Y}\right)^2\right]+\frac{H_a^2E_c}{1+m^2}\left(U^2+W^2\right) \tag{11}$$

$$\bar{\mu} = \left[1 + \left(\tau_D \Big/ \sqrt{\left(\frac{\partial U}{\partial Y}\right)^2 + \left(\frac{\partial W}{\partial Y}\right)^2} \right)^{1/2} \right]^2 \tag{12}$$

Where, $S = \dfrac{\rho v_0 h}{K_c^2}$ (**Suction Parameter**)

$R_e = \dfrac{\rho U_0 h}{K_c^2}$ (**Reynold's Number**)

$H_a^2 = \dfrac{\sigma B_0^2 h^2}{K_c^2}$ (**Hartmann Number Squared**)

$P_r = \dfrac{\rho c_p U_0 h}{\kappa}$ (**Prandtl Number**)

$E_c = \dfrac{U_0 K_c^2}{\rho c_p h (T_2 - T_1)}$ (**Eckert Number**)

$m = \sigma \beta B_0$ (**Hall Parameter**)

$\tau_D = \dfrac{\tau_0 h}{U_0 K_c^2}$ (**Casson Number**)

Also the associated initial (6) and boundary (7) conditions become;

$\tau \le 0, \quad U = 0, \quad W = 0, \quad \theta = 0$ everywhere (13)

$\tau > 0, \quad U = 0, \quad W = 0, \quad \theta = 0$ for $Y = -1$

$U = 1, \quad W = 0, \quad \theta = 1$ for $Y = 1$ (14)

4. Shear Stress and Nusselt Number

The quantities of chief physical interest are shear stress and Nusselt number. From the velocity field, the effects of various parameters on the plate shear stress have been investigated in case of moving plate. The primary shear stress $\tau_x = \mu \left(\dfrac{\partial u}{\partial y} \right)_{y=h}$ and the secondary shear stress $\tau_z = \mu \left(\dfrac{\partial w}{\partial y} \right)_{y=h}$ which are proportional to $\bar{\mu} \left(\dfrac{\partial U}{\partial Y} \right)_{Y=1}$ and $\bar{\mu} \left(\dfrac{\partial W}{\partial Y} \right)_{Y=1}$ respectively. From the

temperature field, the effects of various parameters on Nusselt number in case of moving plate have been calculated. Nusselt number, $N_u = \mu\left(-\frac{\partial T}{\partial y}\right)_{y=h}$ which is proportional to $\bar{\mu}\left(-\frac{\partial \theta}{\partial Y}\right)_{Y=1}$.

5. Numerical Technique

In this section, the governing second order nonlinear coupled dimensionless partial differential equations with the associated initial and boundary conditions are attempted to solve. The explicit finite difference method has been used to solve equations (8)-(12) with the help of the conditions given by (13) and (14). The present problem requires asset of the finite difference equations. In this case the region within the boundary layer is divided by some perpendicular lines of *Y*-axis, where *Y*-axis is normal to the medium as shown in fig.2.

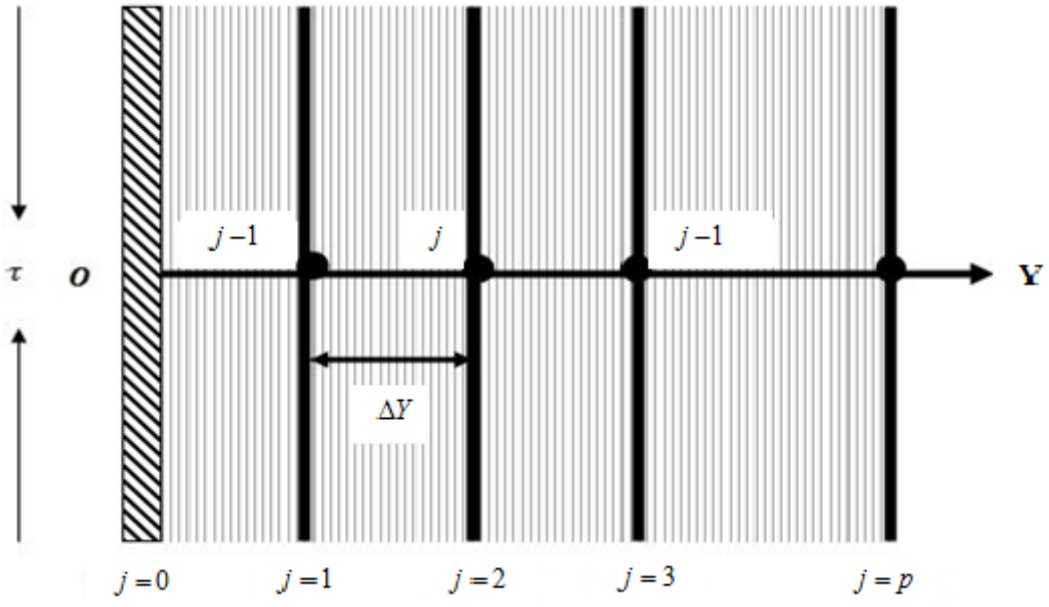

Fig. 2. Finite difference space grid

It is assumed that the maximum length of boundary layer is $Y_{\max}(=2)$ i.e. *Y* varies from -1 to 1 and the number of grid spacing in Y direction is $p(=98)$, hence the constant mesh size along *Y* -axis becomes $\Delta Y = 0.020408(-1 \le y \le 1)$ with a smaller time space $\Delta\tau = 0.0001$.

Let U^{n+1}, W^{n+1} and θ^{n+1} denote the values of U^n, W^n and θ^n at the end of a time-step respectively. Using the explicit finite difference approximation, the set of finite difference equations are obtained as;

$$\frac{U_j^{n+1}-U_j^n}{\Delta\tau}-\frac{S}{R_e}\frac{U_{j+1}^n-U_j^n}{\Delta Y}=-\frac{dP}{dX}+\frac{1}{R_e}\left[\bar{\mu}_j^n\left(\frac{U_{j+1}^n-2U_j^n+U_{j-1}^n}{(\Delta Y)^2}\right)\right]$$

$$+\frac{1}{R_e}\left[\left(\frac{\bar{\mu}_{j+1}^n-\bar{\mu}_j^n}{\Delta Y}\right)\left(\frac{U_{j+1}^n-U_j^n}{\Delta Y}\right)-\frac{H_a^2}{1+m^2}(U_j^n+mW_j^n)\right]$$

$$or,\ \frac{U_j^{n+1}-U_j^n}{\Delta\tau}-\frac{S}{R_e}\frac{U_{j+1}^n-U_j^n}{\Delta Y}=P+\frac{1}{R_e}\left[\bar{\mu}_j^n\left(\frac{U_{j+1}^n-2U_j^n+U_{j-1}^n}{(\Delta Y)^2}\right)\right]$$

$$+\frac{1}{R_e}\left[\left(\frac{\bar{\mu}_{j+1}^n-\bar{\mu}_j^n}{\Delta Y}\right)\left(\frac{U_{j+1}^n-U_j^n}{\Delta Y}\right)-\frac{H_a^2}{1+m^2}(U_j^n+mW_j^n)\right]\quad\left[-\frac{dP}{dX}=P(say)\right] \tag{15}$$

$$\frac{W_j^{n+1}-W_j^n}{\Delta\tau}-\frac{S}{R_e}\frac{W_{j+1}^n-W_j^n}{\Delta Y}=\frac{1}{R_e}\left[\bar{\mu}_j^n\left(\frac{W_{j+1}^n-2W_j^n+W_{j-1}^n}{(\Delta Y)^2}\right)\right]$$

$$+\frac{1}{R_e}\left[\left(\frac{\bar{\mu}_{j+1}^n-\bar{\mu}_j^n}{\Delta Y}\right)\left(\frac{W_{j+1}^n-W_j^n}{\Delta Y}\right)-\frac{H_a^2}{1+m^2}(W_j^n-mU_j^n)\right] \tag{16}$$

$$\frac{\theta_j^{n+1}-\theta_j^n}{\Delta\tau}-\frac{S}{R_e}\frac{\theta_{j+1}^n-\theta_j^n}{\Delta Y}=\frac{1}{P_r}\left(\frac{\theta_{j+1}^n-2\theta_j^n+\theta_{j-1}^n}{(\Delta Y)^2}\right)+E_c\,\bar{\mu}_j^n\left[\left(\frac{U_{j+1}^n-U_j^n}{\Delta Y}\right)^2+\left(\frac{W_{j+1}^n-W_j^n}{\Delta Y}\right)^2\right]$$

$$+\frac{E_c\,H_a^2}{1+m^2}\left[(U_j^n)^2+(W_j^n)^2\right] \tag{17}$$

$$\bar{\mu}_j^n=\left[1+\left(\frac{\tau_D}{\sqrt{\left(\frac{U_{j+1}^n-U_j^n}{\Delta Y}\right)^2+\left(\frac{W_{j+1}^n-W_j^n}{\Delta Y}\right)^2}}\right)^{1/2}\right]^2 \tag{18}$$

and the initial and boundary conditions with the finite difference scheme are;

$$\tau=0,\qquad U_j^0=0,\qquad W_j^0=0,\qquad \theta_j^0=0 \tag{19}$$

$$\tau>0,\qquad U_{-1}^n=0,\qquad W_{-1}^n=0,\qquad \theta_{-1}^n=0$$

$$U_1^n=1,\qquad W_1^n=0,\qquad \theta_1^n=1 \tag{20}$$

Here the subscripts j designates the grid points with Y coordinate and the superscript n represents a value of time, $\tau=n\Delta\tau$ where $n=0,1,2,....$ From the initial condition (19), the

values of U_j^n, W_j^n and θ_j^n are known at $\tau = 0$. At the end of any time-step $\Delta\tau$, the new primary velocity U_j^{n+1} the new secondary velocity W_j^{n+1} and the new temperature T_j^{n+1}, at all interior nodal points may be obtained by successive applications of equations (15), (16) and (17) respectively. This process is repeated in time and provided the time-step is sufficiently small U_j^n, W_j^n and θ_j^n should eventually converge to values which approximate the steady-state solution of equations (9)-(11). Also the numerical values of the Shear Stress and Nusselt number are evaluated by five-point approximate formula for the derivative.

6. Stability and convergence analysis

Here an explicit finite difference method is being used; the analysis will remain incomplete unless the stability and convergence of the finite difference scheme are discussed. For the constant mesh sizes the stability criteria of the scheme may be established as follows. The general terms of the Fourier expansion for U, W and θ at a time arbitrarily called $t = 0$ are all $e^{i\alpha Y}$, apart from a constant, where $i = \sqrt{-1}$. At a time $t = \tau$, these terms become;

$$\begin{aligned} U &: \quad \psi(\tau)e^{i\alpha Y} \\ W &: \quad \eta(\tau)e^{i\alpha Y} \\ \theta &: \quad \xi(\tau)e^{i\alpha Y} \\ \bar{\mu} &: \quad \varphi(\tau)e^{i\alpha Y} \end{aligned} \tag{21}$$

and after the time-step these terms will become;

$$\begin{aligned} U &: \quad \psi'(\tau)e^{i\alpha Y} \\ W &: \quad \eta'(\tau)e^{i\alpha Y} \\ \theta &: \quad \xi'(\tau)e^{i\alpha Y} \\ \bar{\mu} &: \quad \varphi'(\tau)e^{i\alpha Y} \end{aligned} \tag{22}$$

Substituting (21) and (22) into equations (15)-(17), the stability conditions of the problem are as furnished below;

$$\frac{\Delta\tau}{\Delta Y}\frac{S}{R_e} + \frac{\Delta\tau}{2R_e}\frac{H_a^2}{1+m^2} \le 1 \quad \text{and} \tag{23}$$

$$\frac{\Delta\tau}{\Delta Y}\frac{S}{R_e}+\frac{2\Delta\tau}{(\Delta Y)^2}\frac{1}{P_r}\le 1 \qquad (24)$$

From equations (23) and (24) the convergence criteria of the problem are $R_e \ge 0.00223$, $H_a \le 199$, $S \le 500$ and $P_r \ge 0.081$.

7. Results and Discussion

In this section, it has been presented that the results obtained using the successive explicit finite difference numerical technique. To investigate the physical conditions of the developed mathematical model it has been obtained the numerical values of the x and z components of velocity, commonly known as primary and secondary velocity and temperature within the boundary layer for the laminar boundary layer flow.

In order to analyze the physical situation of the model, it has been computed the steady state numerical values of the non-dimensional primary velocity U, secondary velocity W, temperature θ, shear stress τ and Nusselt number N_u within the boundary layer for different values of Suction parameter(S), Reynold's number(R_e), Hall parameter(m), Hartmann number(H_a), Prandtal number(P_r) and Eckert number(E_c) with the fixed value of Casson number(τ_D).

The transient primary velocity, secondary velocity, temperature profiles, steady state shear stress and Nusselt number have been shown in Figs. 4.3 to 4.38 for different values of S, R_e, m, H_a, P_r and E_c. The values of S, R_e, m, H_a, P_r and E_c are chosen arbitrarily.

In case of Suction parameter S ;

The effects of the Suction parameter S on the primary velocity, secondary velocity, temperature field, primary shear stress, secondary shear stress and Nusselt number are presented in Figs. 4.3 to 4.8 respectively.

It has been observed that primary velocity U increases with the increase of Suction parameter S in Fig. 4.3. At first the secondary velocity W increases then decreases with the increase of Suction parameter S, that means secondary velocity profile is a cross flow in Fig. 4.4. Figs. 4.5-4.8 represent the temperature profile θ, primary shear stress τ_x, secondary shear stress τ_z and Nusselt number N_u increase for the increasing values of S.

In case of Reynold's number R_e ;

The effects of the Reynold's number R_e on the primary velocity, secondary velocity, temperature field, primary shear stress, secondary shear stress and Nusselt number are presented in Figs. 4.9 to 4.14 respectively.

It has been observed that the primary velocity U, secondary velocity W, primary shear stress τ_x and secondary shear stress τ_z have increased gradually as the rise of R_e as illustrated in Figs. 4.9, 4.10, 4.12 and 4.13 respectively.

The temperature profile θ and Nusselt number N_u have decreased with the increasing values of R_e shown in Figs. 4.11 and 4.14 respectively.

In case of Prandtl number P_r ;

The primary velocity U, secondary velocity W, primary shear stress τ_x and secondary shear stress τ_z are unchanged with the rise of Prandtl number P_r as shown in Figs. 4.15, 4.16, 4.18 and 4.19 respectively. T

he temperature profile θ and Nusselt number N_u have increased with the increasing values of Prandtl number P_r shown in Figs. 4.17 and 4.20 respectively.

In case of Hall parameter m ;

The effects of the Hall parameter m on the primary velocity, secondary velocity, temperature field, primary shear stress, secondary shear stress and Nusselt number are presented in Figs. 4.21 to 4.26 respectively.

It has been observed that the primary velocity U, secondary velocity W, primary shear stress τ_x and secondary shear stress τ_z have increased as the rise of m as illustrated in Figs. 4.21, 4.22, 4.24 and 4.25 respectively.

The negligible effect of m on temperature profile θ has been found with the increasing values of m shown in Fig. 4.23. The Nusselt number N_u increases with the increase of m as shown in Fig. 4.26.

In case of Hartmann number H_a ;

The effects of the Hartmann number H_a on the primary velocity, secondary velocity, temperature field, primary shear stress, secondary shear stress and Nusselt number are presented in Figs. 4.27 to 4.32 respectively.

The primary velocity U and primary shear stress τ_x have decreased with the increase of Hartmann number H_a as shown in Figs. 4.27 and 4.30 respectively. At first the secondary velocity W increases thereafter decreases with the increase of Hartmann number H_a, that means secondary velocity profile is a cross flow in Fig. 4.28. It is observed from Fig. 4.31, the secondary shear stress τ_z decreases with the increase of Hartmann number H_a.

The negligible effect of H_a on temperature profile θ has been found with the increasing values of H_a shown in Fig. 4.29. The Nusselt number N_u decreases with the increase of H_a as shown in Fig. 4.32.

In case of Eckert number E_c ;

The effects of the Eckert number E_c on the primary velocity, secondary velocity, temperature field, primary shear stress, secondary shear stress and Nusselt number are presented in Figs. 4.33 to 4.38 respectively

It has been observed that the primary velocity U, secondary velocity W, primary shear stress τ_x and secondary shear stress τ_z are unchanged with the rise of Eckert number E_c as shown in Figs. 4.33, 4.34, 4.36 and 4.37 respectively.

The temperature profile θ and Nusselt number N_u have increased with the increasing values of Eckert number E_c as shown in Figs. 4.35 and 4.38 respectively. Hence it is concluded that the maximum velocity occurs in the vicinity of the plate.

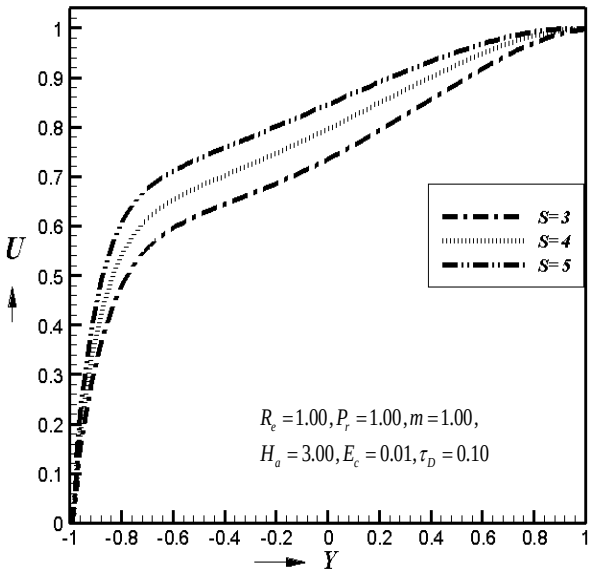

Fig. 4.3 Primary Velocity Profiles for different values of Dimensionless Suction Parameter ***S***

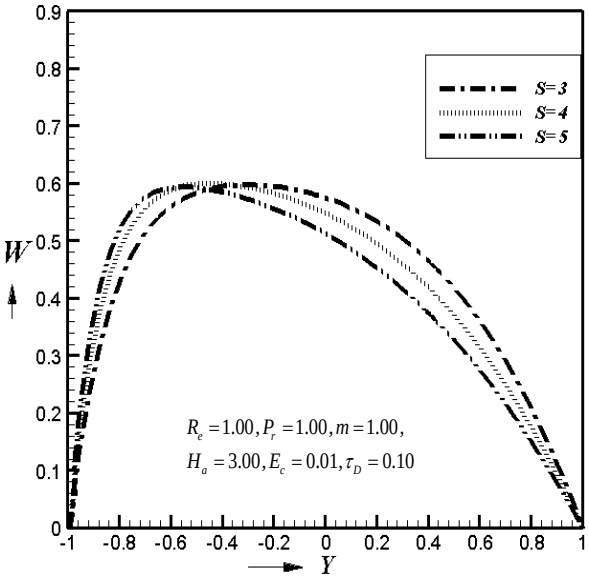

Fig.4.4 Secondary Velocity Profiles for different values of Dimensionless Suction Parameter ***S***

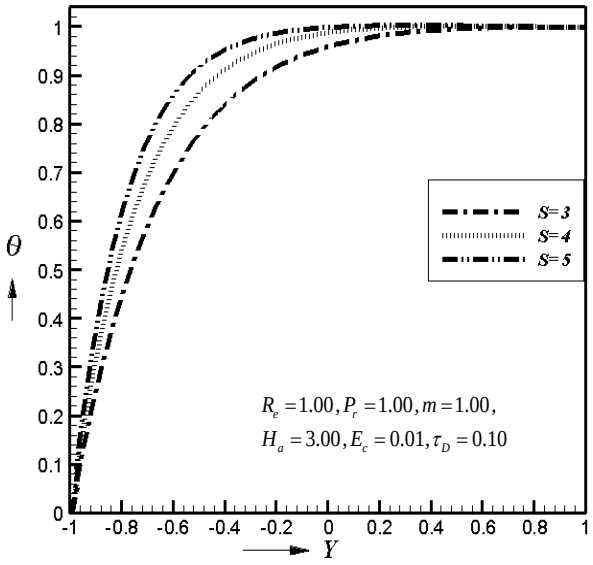

Fig.4.5 Temperature Profiles for different values of Dimensionless Suction Parameter ***S***

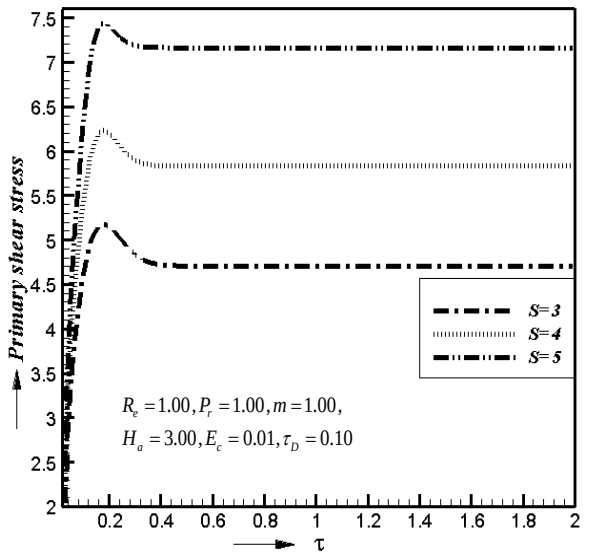

Fig.4.6 Primary Shear Stress τ_x Suction Parameter ***S*** in case of moving plate

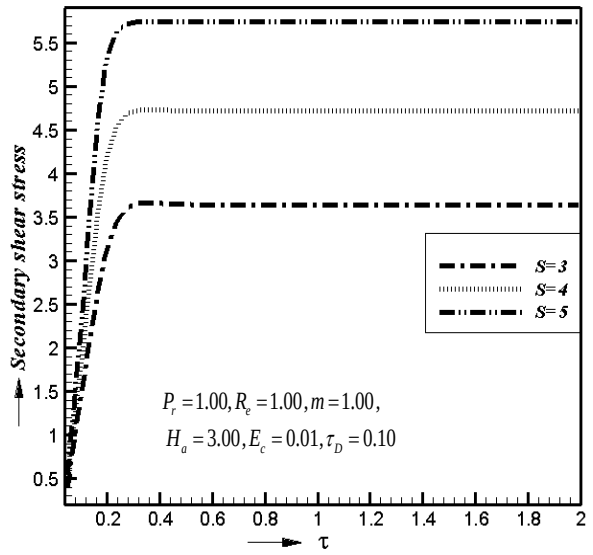

Fig.4.7 Secondary Shear Stress τ_z for Suction Parameter ***S*** in case of moving plate

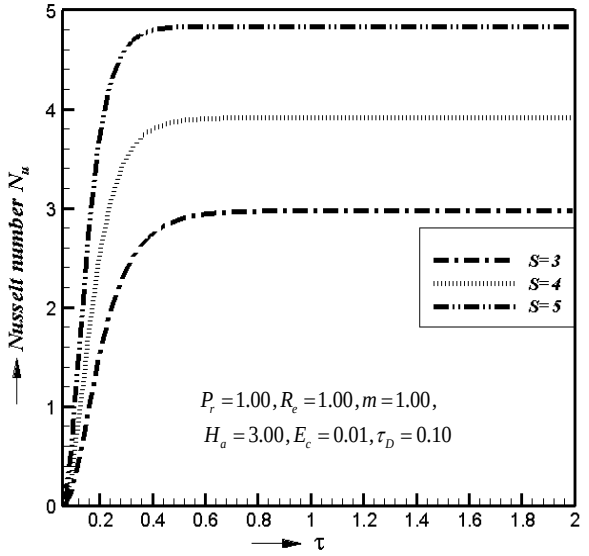

Fig.4.8 Nusselt Number N_u for Suction Parameter ***S*** in case of moving plate

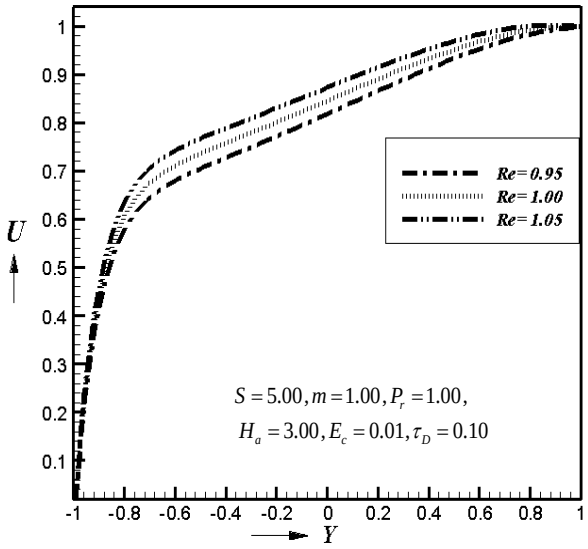

Fig.4.9 Primary Velocity Profiles for different values of Dimensionless Reynolds Number R_e

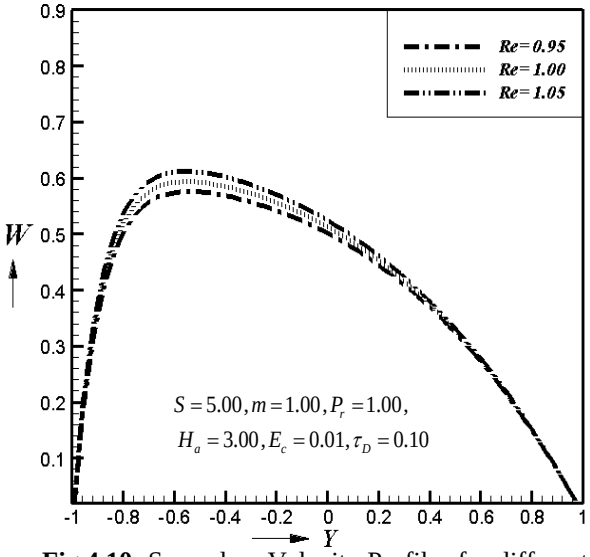

Fig.4.10 Secondary Velocity Profiles for different values of Dimensionless Reynolds Number R_e

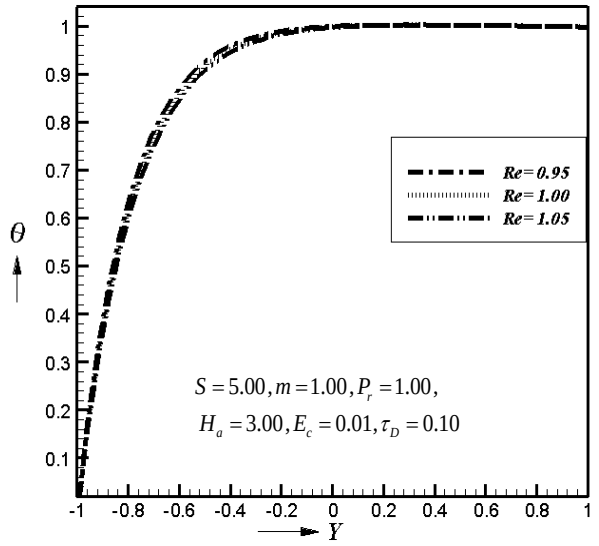

Fig.4.11 Temperature Profiles for different values of Dimensionless Reynolds Number R_e

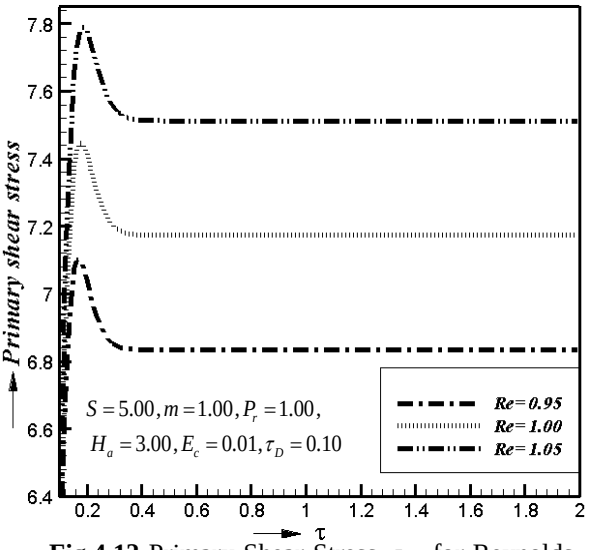

Fig.4.12 Primary Shear Stress τ_x for Reynolds Number R_e in case of moving plate

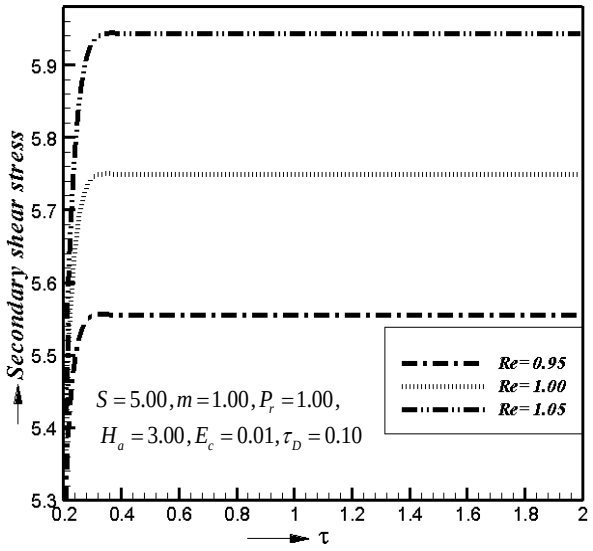

Fig.4.13 Secondary Shear Stress τ_z for Reynolds Number R_e in case of moving plate

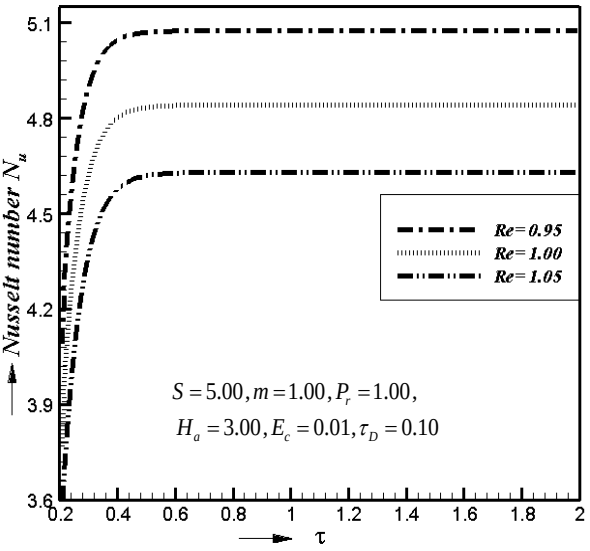

Fig.4.14 Nusselt Number N_u for Reynolds Number R_e in case of moving plate

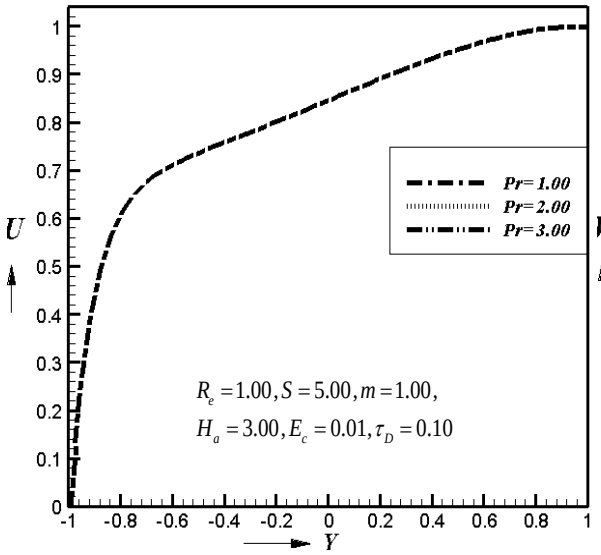

Fig.4.15 Primary Velocity Profiles for different values of Dimensionless Prandtl Number P_r

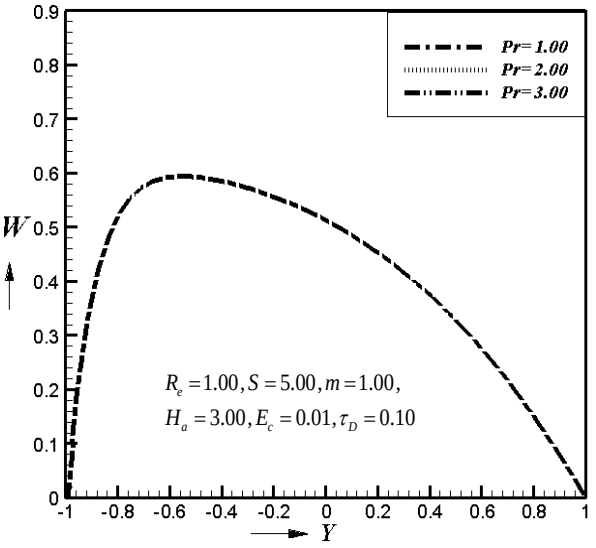

Fig.4.16 Secondary Velocity Profiles for different values of Dimensionless Prandtl Number P_r

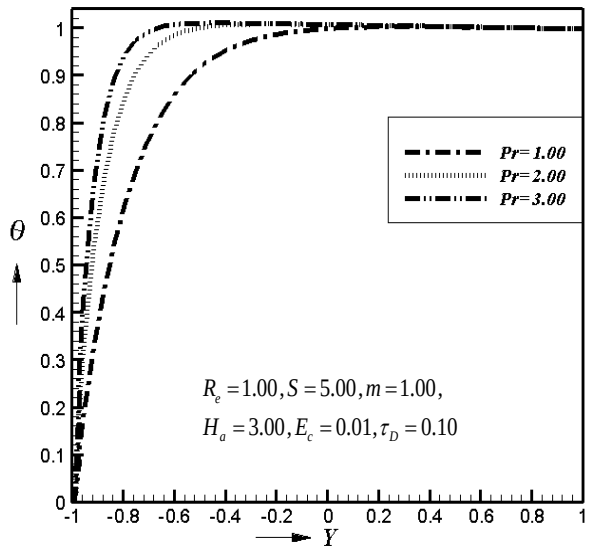

Fig.4.17 Temperature Profiles for different values of Dimensionless Prandtl Number P_r

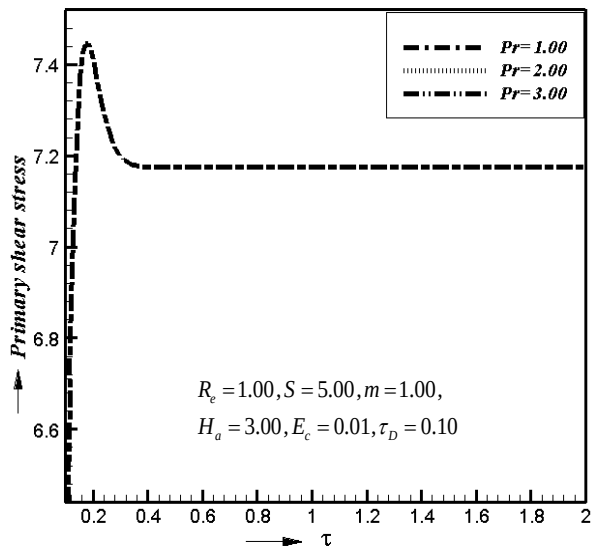

Fig.4.18 Primary Shear Stress τ_x for Prandtl Number P_r in case of moving plate

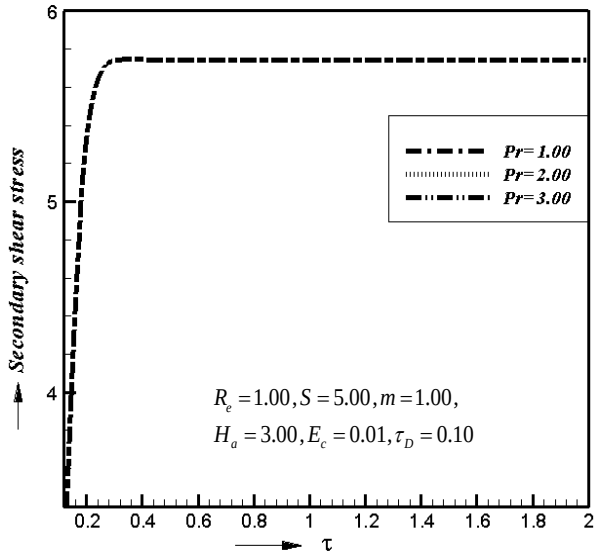

Fig.4.19 Secondary Shear Stress τ_z for Prandtl Number P_r in case of moving plate

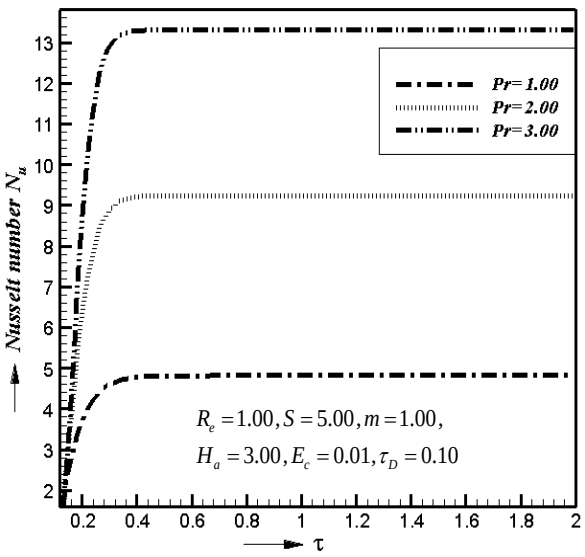

Fig.4.20 Nusselt Number N_u for Prandtl Number P_r in case of moving plate

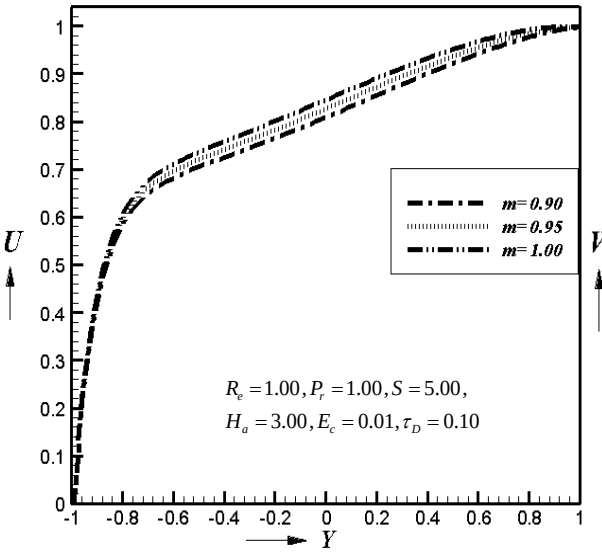

Fig.4.21 Primary Velocity Profiles for different values of Dimensionless Hall Parameter ***m***

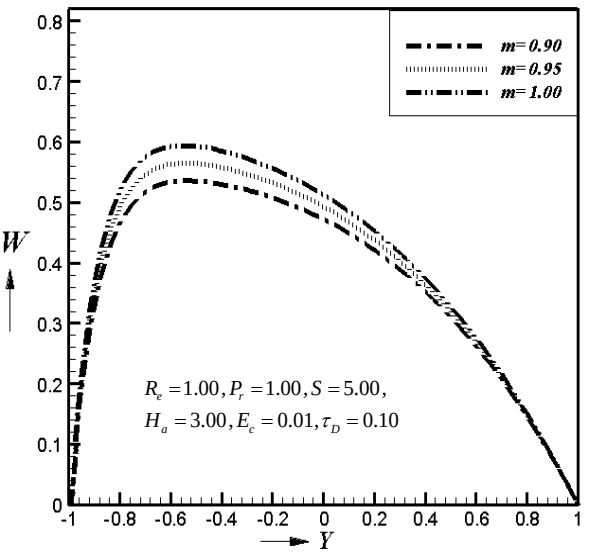

Fig.4.22 Secondary Velocity Profiles for different values of Dimensionless Hall Parameter ***m***

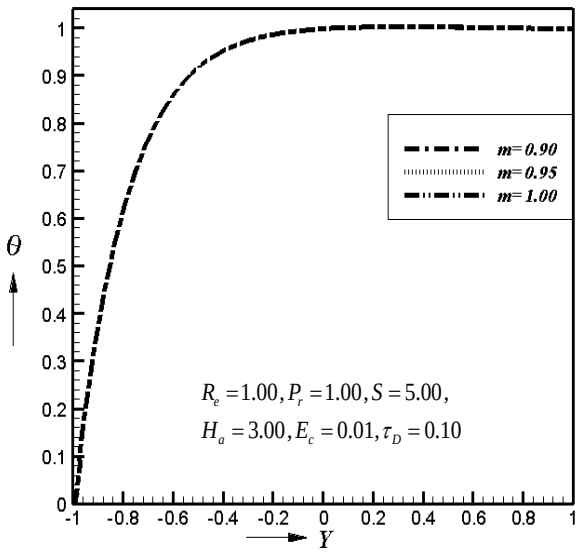

Fig.4.23 Temperature Profiles for different values of Dimensionless Hall Parameter ***m***

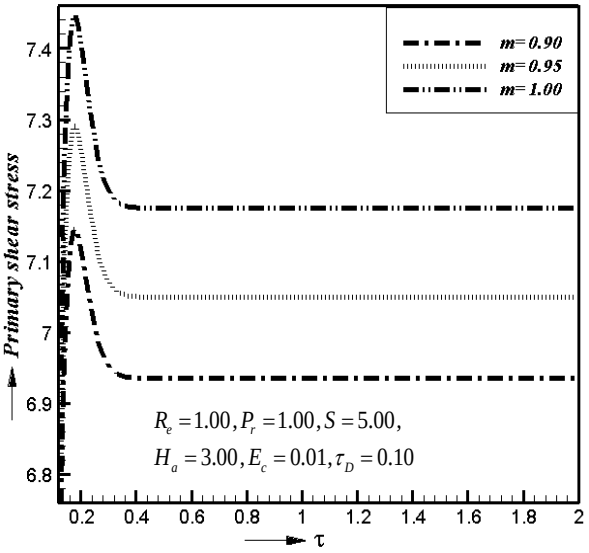

Fig.4.24 Primary Shear Stress τ_x for Hall Parameter ***m*** in case of moving plate

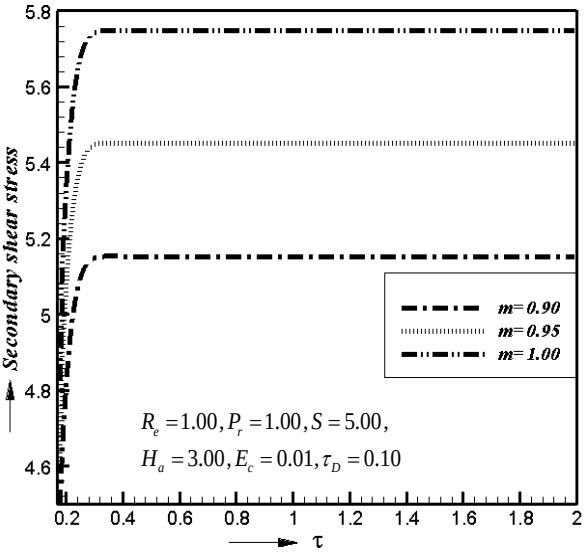

Fig.4.25 Secondary Shear Stress τ_z for Hall Parameter ***m*** in case of moving plate

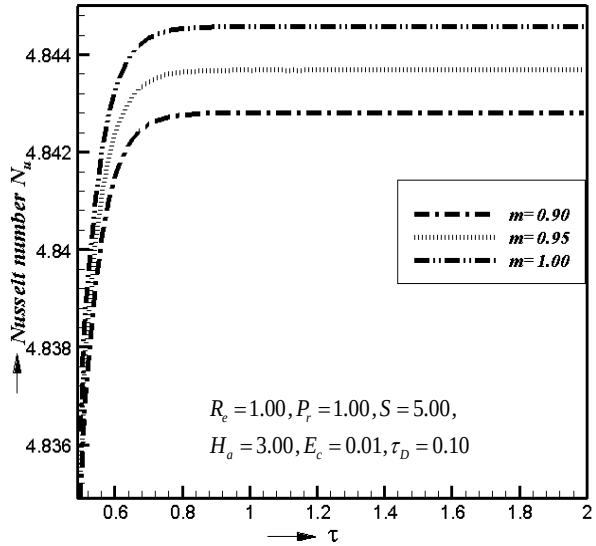

Fig.4.26 Nusselt Number N_u for Hall Parameter ***m*** in case of moving plate

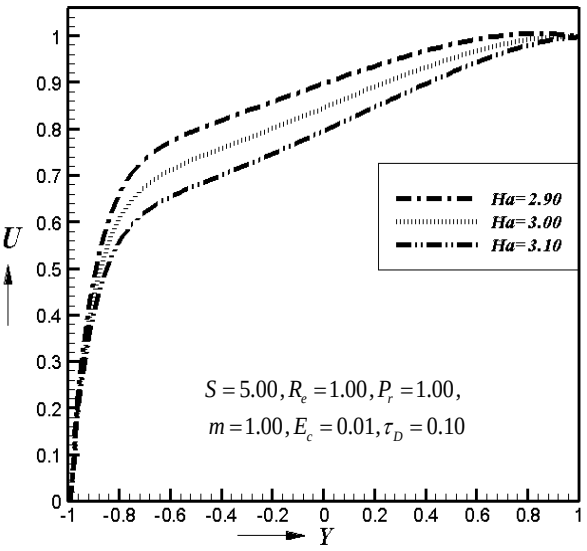

Fig.4.27 Primary Velocity Profiles for different values of Dimensionless Hartmann Number H_a

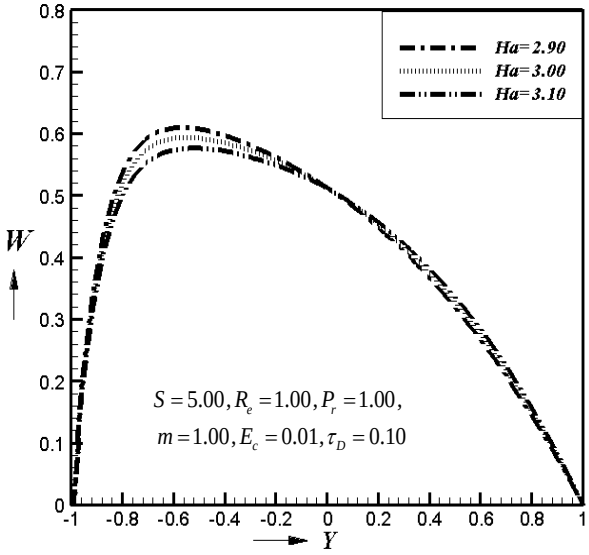

Fig.4.28 Secondary Velocity Profiles for different values of Dimensionless Hartmann Number H_a

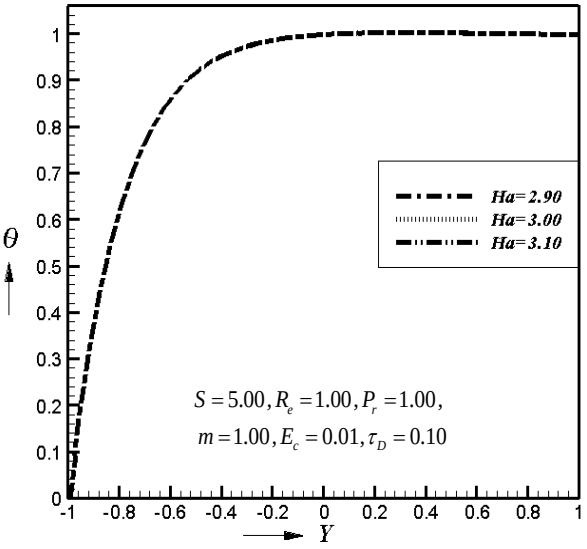

Fig.4.29 Temperature Profiles for different values of Dimensionless Hartmann Number H_a

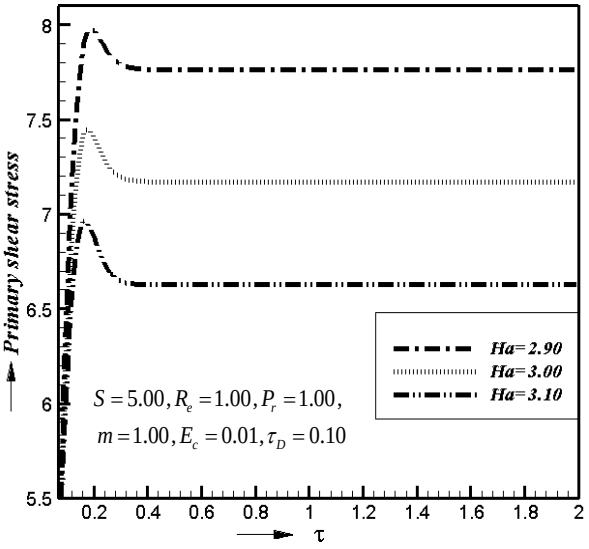

Fig.4.30 Primary Shear Stress τ_x for Hartmann Number H_a in case of moving plate.

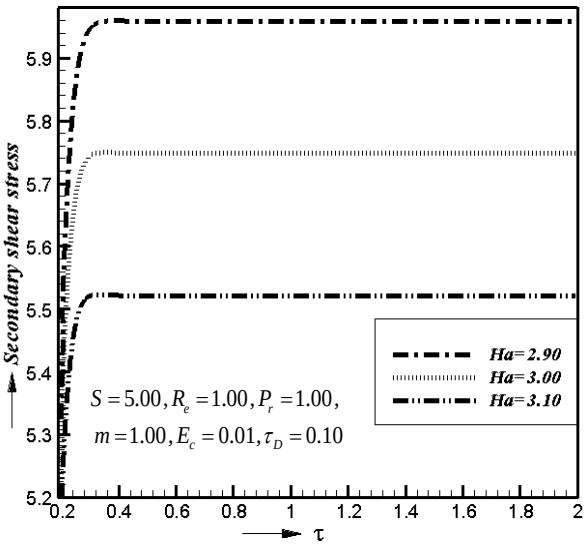

Fig.4.31 Secondary Shear Stress τ_z for Hartmann Number H_a in case of moving plate

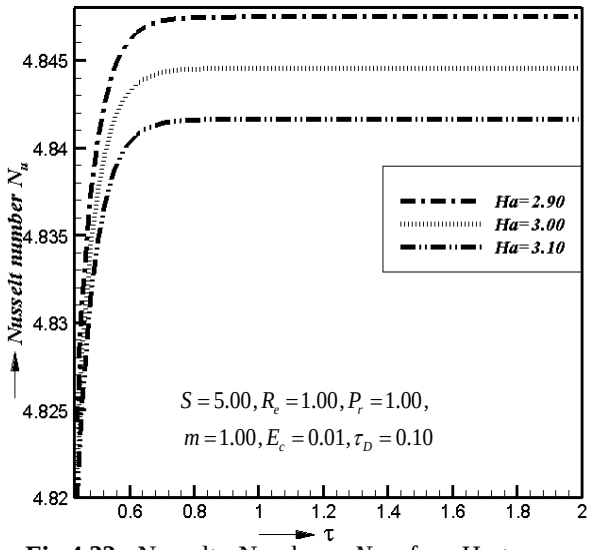

Fig.4.32 Nusselt Number N_u for Hartmann Number H_a in case of moving plate

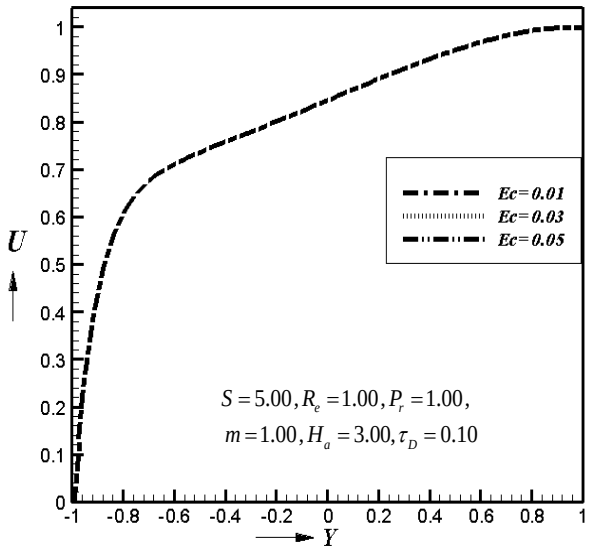

Fig.4.33 Primary Velocity Profiles for different values of Dimensionless Eckert Number E_c

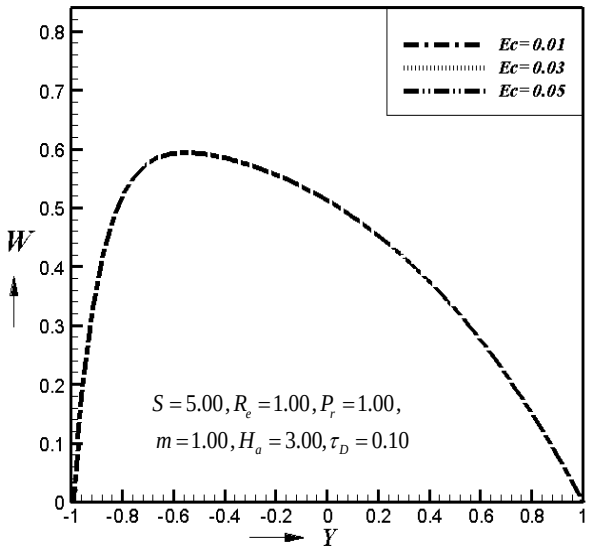

Fig.4.34 Secondary Velocity Profiles for different values of Dimensionless Eckert Number E_c

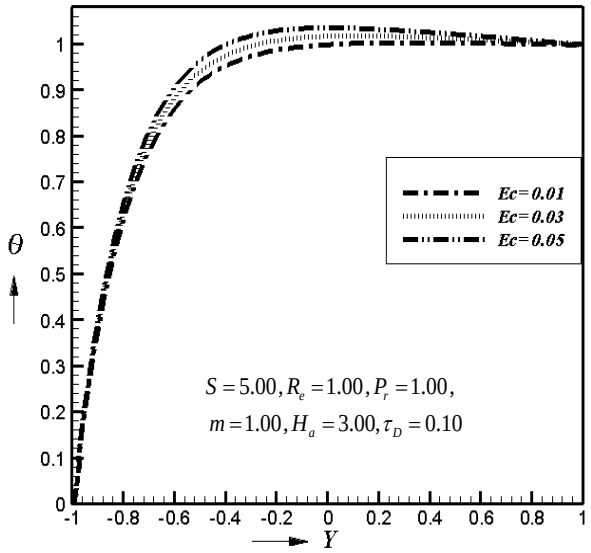

Fig.4.35 Temperature Profiles for different values of Dimensionless Eckert Number E_c

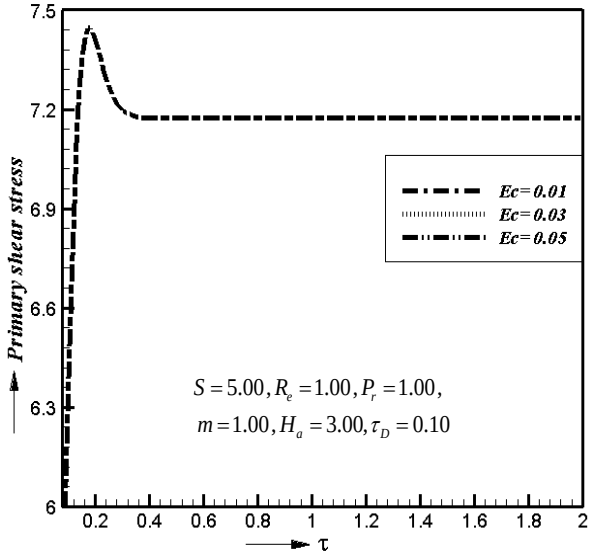

Fig.4.36 Primary Shear Stress τ_x for Eckert Number E_c in case of moving plate

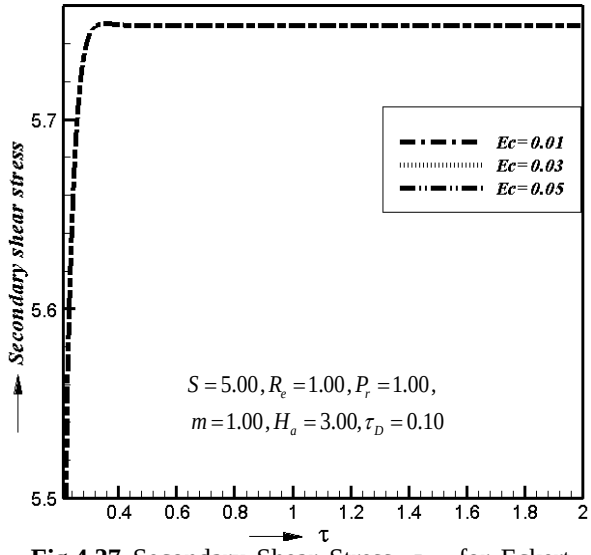

Fig.4.37 Secondary Shear Stress τ_z for Eckert Number E_c in case of moving plate

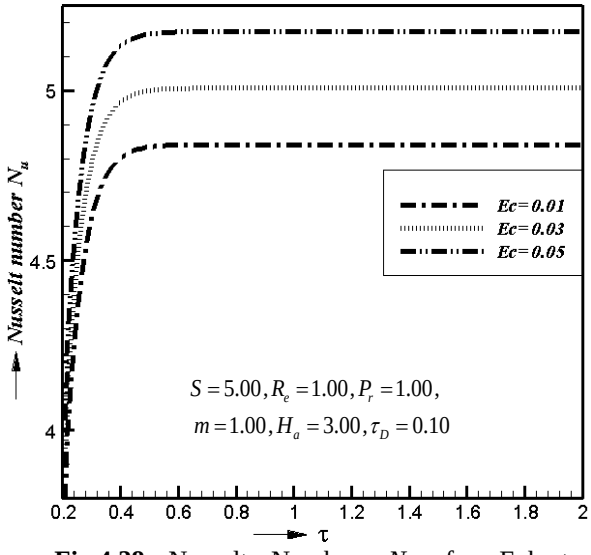

Fig.4.38 Nusselt Number N_u for Eckert Number E_c in case of moving plate

8. Conclusions

In this study, the required physical problem has been studied mathematically for differential perspectives, mostly concerned with their solutions. The coupled partial differential equations have been solved numerically by explicit finite difference technique. The unsteady magnetohydrodynamic flow of an electrically conducting viscous incompressible non-Newtonian Casson fluid bounded by parallel non-conducting porous plates has been studied with Hall current, Joule heating and Viscous dissipation.

The results are discussed for different values of important dimensionless parameters as Suction parameter (S), Reynold number (R_e), Hall parameter (m), Prandtal number (P_r), Hartmann number (H_a) and Eckert number (E_c) with the fixed value of Casson number (τ_D). Some of the important findings obtained from the graphical representation of the results are listed herewith;

1. The primary velocity increases with the increase of S , R_e and m. It decreases with the increase of H_a and no change for P_r and E_c.
2. The secondary velocity increases with the increase of R_e and m. It shows the cross flow with the increase of S and H_a and no change for P_r and E_c.
3. The temperature increases with the increase of S, P_r and E_c. It decreases with the increase of R_e and shows the minor effect with the increase of m and H_a .
4. The primary shear stress in case of moving plate increases with the increase of S , R_e, and m . It decreases with the increase of H_a and no change for P_r and E_c.
5. The secondary shear stress in case of moving plate increases with the increase of S , R_e, and m. It decreases with the increase of H_a and no change for P_r and E_c.
6. The Nusselt number in case of moving plate increases with the increase of S , E_c, P_r and m while it decreases with the increase of R_e and H_a.

As the basis for many scientific and engineering applications for studying more complex problems involving the flow of electrically conducting fluids, it is hoped that the present investigation of the study of applied physics of flow through the parallel plates can be utilized. In the purification of crude oil and fluid droplets and sprays as well as in the polymer processing

industries and biomechanics, the findings may be useful for study of movement and flow of shear thinning liquids. This work has been done for academic point of view.

References

1. N. Casson "A Flow Equation for Pigment Oil-Suspensions of the Printing Ink Type", in Rheolgy of Disperse Systems (C.C. Mill, Ed.), Pergamon Press, London, p. 84, 1959.
2.. W.P. Walawander, T.Y. Chen and D.F. Cala "An Approximate Casson Fluid Model for Tube Flow of Blood", *Biorheology*, vol. 12, no.2, pp. 111-124, 1975.
3. R.L. Batra, and B. Jena "Flow of a Casson Fluid in a Slightly Curved Tube", *International Journal of Engineering Science.*, vol. 29, no. 10, pp. 1245-1258, 1991.
4. B. Das and R.L. Batra "Secondary Flow of a Casson Fluid in a Slightly Curved Tube", *International Journal of Non-Linear Mechanics*, vol. 28, no. 5, pp. 567-577, 1993.
5. M.E. Sayed-Ahmed and H.A. Attia "Magnetohydrodynamic Flow and Heat Transfer of a Non-Newtonian Fluid in an Eccentric Annulus", *Canadian Journal of Physics*, vol. 76, no. 5, pp. 391-401, 1998.
6. H.A. Attia and M.E. Sayed-Ahmed "Hydrodynamic Impulsively Lid-Driven Flow and Heat Transfer of a Casson Fluid", *T. Journal of Science and Engineering*, vol. 9, no. 3, pp. 195-204, 2006.
7. S.N. Sahoo, J.P. Panda and G.C. Dash "The MHD mixed convection stagnation point flow and heat transfer in a porous medium", *Proceedings of Natural Academic Science*, vol. 83, no. 4, pp. 371-381. 2013.
8. J.P. Panda, N. Dash and G.C. Dash "Heat and mass transfer on MHD flow through porous media over an accelerating surface in the presence of suction and blowing", *Journal of Engineering Thermophysics*, vol. 21, no. 2, pp. 119-13, 2012.
9. J.P. Panda, N. Dash, G.C. Dash "Hydromagnetic flowand heat transfer through porous medium of elasto-viscous fluid over a porous plate in the slip flow regime", *AMSE Journals*, series Modelling B, vol. 80, no. 1-2, pp. 71-87, 2011.
10. H.A. Attia "Hall Current Effects on the Velocity and Temperature Fields of an Unsteady Hartmann Flow", *Canadian Journal of Physics*, vol. 76, no. 9, pp. 739-746, 1998.

11. H.A. Attia and M.E. Sayed-Ahmed "Transient MHD Couette Flow of a Casson Fluid between Parallel Plates with Heat Transfer", *Italian Journal of pure and applied Mathematics*, no. 27, pp. 19-38, 2010.
12. M.E. Sayed-Ahmed, H.A. Attia, and K.M. Ewis "Time Dependent Pressure Gradient Effect on Unsteady MHD Couette Flow and Heat Transfer of a Casson Fluid", *Canadian Journal of Physics*, vol. 3, no.1 pp. 38-49, 2011.